Polymer 49 (2008) 3462–3469

Contents lists available at ScienceDirect

Polymer

journal homepage: www.elsevier.com/locate/polymer

Efficiency of graft copolymers at stabilizing co-continuous polymer blends during quiescent annealing

Cai-Liang Zhang [a,b], Lian-Fang Feng [a,*], Jian Zhao [a], Hua Huang [c], Sandrine Hoppe [b], Guo-Hua Hu [b,d,**]

[a] State Key Laboratory of Chemical Engineering, College of Materials Science and Chemical Engineering, Zhejiang University, Hangzhou 310027, China
[b] Laboratory of Chemical Engineering Sciences, Nancy Université, CNRS-ENSIC-INPL, 1 rue Grandville, BP 20451, 54001 Nancy, France
[c] Material Science Pacific, Dow Chemical (China) Company, 512 Yutang Road, Shanghai 201613, China
[d] Institut Universitaire de France, Maison des Universités, 103 Boulevard Saint-Michel, 75005 Paris, France

ARTICLE INFO

Article history:
Received 6 April 2008
Received in revised form 1 June 2008
Accepted 3 June 2008
Available online 7 June 2008

Keywords:
Quiescent annealing
Co-continuous morphology
Graft copolymer

ABSTRACT

This work was aimed at studying the efficiency of graft copolymers at stabilizing the co-continuous morphology of polystyrene (PS)/polyamide 6 (PA6) blends during quiescent annealing. A series of graft copolymers with PS as backbone and PA6 as grafts, denoted as PS-*g*-PA6, with different molecular structures and compositions were used as compatibilizers. The co-continuous domain size of the blends without PS-*g*-PA6 increased almost linearly with annealing time. The addition of the PS-*g*-PA6 not only narrowed down the composition range of co-continuity of PS/PA6 blend but also slowed down and even stopped completely the coarsening of the co-continuous morphology during the quiescent annealing. Moreover, the efficiency of PS-*g*-PA6 depended very much on its molecular structure and/or composition. For graft copolymers with similar backbone and graft chain number, the longer the grafts, the higher their stabilizing efficiency. For a given backbone/graft composition, graft copolymers having fewer and longer grafts were more efficient at compatibilizing and stabilizing the co-continuous morphology.

1. Introduction

It is common practice to create new polymer materials with desirable properties by blending different polymers. In a two-phase polymer blend, two types of morphologies can be encountered: disperse/matrix and co-continuous morphology. In general, at low concentration of one phase, the morphology is the former; increasing the concentration of the minor phase leads to the latter; at higher concentrations phase inversion leads once again to disperse/matrix morphology. The type of morphology depends not only on their volume fractions but also on the nature of the polymers (interfacial tension [1], viscosity ratio [2,3] and interface type [4]), and processing conditions [5]. Due to their interconnected nature, co-continuous morphologies have the potential to significantly widen the application range of polymer blends [6–8]. Therefore, recently there has been significant interest in polymer blends with co-continuous morphology [9–24].

Many studies [11–15] have focused on the stability of co-continuous morphologies under quiescent annealing conditions. On the one hand, below a critical volume fraction of the minor component, the co-continuous morphology may evolve into a dispersed morphology at isothermal annealing, implying a narrowing of the co-continuous range [11–13]. On the other hand, co-continuous morphologies can undergo significant coarsening effects under quiescent annealing condition. Yuan and Favis [14,15] found that the domain diameter increased linearly with annealing time at all annealing temperatures and for all the co-continuous polystyrene (PS)/polyethylene (PE) blends.

Block or graft copolymers whose segments are chemically identical to or have affinity with the polymer components are often used as compatibilizers (also called interfacial modifiers or emulsifiers) to reduce the interfacial tension, promote the dispersion of one phase in another and stabilize resulting blends [16–18]. Several studies have investigated the effect of block copolymer on the boundaries of the region of co-continuity [19–21] and the morphologies' stability of co-continuous polymer blends during quiescent annealing [15,22–24]. In each case, the addition of block copolymer narrowed down the composition range of co-continuity. Table 1 gathers some literature results on the effects of the molar mass and molecular architecture of a block copolymer on its efficiency at stabilizing the co-continuous morphology of polymer blends during quiescent annealing. The efficiency of block copolymer followed the order: tapered diblock > conventional diblock > triblock; an intermediate molar mass was the most efficient.

* Corresponding author.
** Corresponding author. Laboratory of Chemical Engineering Sciences, Nancy Université, CNRS-ENSIC-INPL, 1 rue Grandville, BP 20451, 54001 Nancy, France. Tel.: +33 383175339; fax: +33 383322975.
E-mail addresses: fenglf@zju.edu.cn (L.-F. Feng), hu@ensic.inpl-nancy.fr (G.-H. Hu).

0032-3861/$ – see front matter © 2008 Elsevier Ltd. All rights reserved.
doi:10.1016/j.polymer.2008.06.003

Table 1
Literature results on the efficiency of copolymers to stabilize co-continuous morphology

Blend	Type of copolymer	Effect of the copolymer
PS/PE (80/20) [23,24]	Diblock: PS-*b*-PB (35-35 kg/mol; 50% PS); tapered diblock: PS-*b*-P(S-*co*-B)-*b*-PB (23-19-28 kg/mol, 50% PS); triblock: PS-*b*-P(S-*co*-B)-*b*-PS (7.5-35-7.5 kg/mol, 30% PS)	The tapered diblock copolymer was the most efficient. The superiority of the tapered diblock over the diblock and triblock might be due to its ability to quantitatively locate at the interface
PS/PE (50/50) [15]	Diblock: SEB (33.4-29.6 kg/mol; 53% PS); triblock: SEBS (7.5-35-7.5 kg/mol, 30% PS)	The diblock copolymer was more efficient in the suppression of the coarsening effect. The triblock had higher tendency to form micelles
PS/PE (50/50) [19]	Four symmetric PS–PE diblock with molar masses of 6, 40, 100 and 200 kg/mol	An intermediate molar mass PS–PE, 40 kg/mol, was most efficient. The existence of a copolymer with an optimal molar mass was due to a balance between the ability of copolymer to reach the interface and its relative stabilization effect at the interface

The aforementioned studies are mainly focused on the efficiency of block copolymers. The work reported in this paper was aimed at studying the efficiency of graft copolymers with different molecular structures and compositions at stabilizing co-continuous morphology under quiescent annealing with emphasis on the length and density of grafts. The blend system was composed of PS and polyamide 6 (PA6). A series of the graft copolymer PS-*g*-PA6 with different molecular structures and/or molar masses were used as compatibilizers.

2. Experimental

2.1. Materials

Table 2 shows selected characteristics of PS and PA6 used in this work. The PS-*g*-PA6 graft copolymers were obtained by the anionic polymerization of ε-caprolactam onto a random copolymer of styrene (St) and 3-isopropenyl-α,α-dimethylbenzene isocyanate (TMI), denoted as PS-*co*-TMI. Details on the polymerization principle and procedures can be found elsewhere [25–27]. Table 3 shows some of the characteristics of the PS-*co*-TMI used for the polymerization. TMI contents in PS-*co*-TMI were measured following a method reported in the literature [28].

Table 2
Selected characteristics of the PS and PA6 used in this work

	Number average molar mass[a] (M_n) (kg/mol)	Mass average molar mass[a] (M_w) (kg/mol)	Supplier
PS	101.3	228.8	Yangzi-BASF Styrenics Co., Nanjing, China
PA6	19.4	49.4	UBE Nylon Ltd., Thailand

[a] Molar masses measured by size exclusion chromatography (SEC) using PS standards for the calibration and tetrahydrofuran (THF) as the eluent. The PA6 was first *N*-trifluoroacetylated before the SEC measurement [25].

Table 3
Selected characteristics of the copolymer PS-*co*-TMI

PS-*co*-TMI	M_n[a] (kg/mol)	M_w[a] (kg/mol)	TMI content in PS-*co*-TMI[b] (wt.%)
PS-*co*-TMI2	34.7	68.0	2
PS-*co*-TMI4	33.3	97.0	4

[a] Molar masses measured by SEC using PS standards for the calibration and THF as the eluent.
[b] TMI contents were measured following a method reported in the literature [28].

The isocyanate moieties of the PS-*co*-TMI acted as initiating centers from which PA6 chains grew in the presence of a catalyst like sodium caprolactam (NaCL). Table 4 shows selected characteristics of four as-synthesized PS-*g*-PA6 graft copolymers used in this work. The first three graft copolymers had the same PS backbone and the same number of PA6 grafts with different lengths. The fourth graft copolymer, PS-*g*-PA6d, differed from the first three in that the number of the PA6 grafts per PS backbone was not 6.6 but 3.4. Its graft length was almost the same as that of PS-*g*-PA6c and almost twice that of PS-*g*-PA6b.

2.2. Blend preparation

Polymer blends were prepared by mixing the components in a Haake batch mixer (HBI system 90) equipped with a mixing chamber and two rotors inside the mixing chamber. For the compatibilized blend systems, the concentration of the as-synthesized PS-*g*-PA6 graft copolymer in the blends was 1% with respect to the PS/PA6 blends. Prior to the blending, the PS, PA6 and PS-*g*-PA6 were dried in a vacuum oven at 80 °C for 12 h. The dried blend components were charged simultaneously into the mixing chamber and were mixed at 100 rpm and 230 °C for 10 min. Samples were taken from the mixing chamber and then quenched in liquid nitrogen to freeze-in their morphologies.

2.3. Quiescent annealing

Pieces of blend samples of about 20 mm thick were warped with coppery netting and then annealed in a silicon oil bath that was preheated to 230, 235 or 240 °C. After various annealing times (from 2 to 20 min), they were taken out from the oil-bath and then quenched immediately in liquid nitrogen to freeze-in the morphologies.

Table 4
Selected characteristics of the as-synthesized PS-*g*-PA6 graft copolymers

Copolymer designation[a]	Composition of PS-*g*-PA6		Number of PA6 grafts per PS backbone	M_n (kg/mol)		
	PS backbone	PA6 grafts		PS backbone	Each PA6 graft	PS-*g*-PA6[b]
PS-*g*-PA6a	75.3	24.7	6.6	33.3	1.7	34.9
PS-*g*-PA6b	69.4	30.6	6.6	33.3	2.2	38.1
PS-*g*-PA6c	49.7	50.3	6.6	33.3	5.1	47.1
PS-*g*-PA6d	69.2	30.8	3.4	36.9	4.8	36.0

[a] PS-*g*-PA6a, PS-*g*-PA6b and PS-*g*-PA6c were synthesized using PS-*co*-TMI4 and PS-*g*-PA6d using PS-*co*-TMI2.
[b] Molar masses measured by SEC using PS standards for the calibration and THF as the eluent. PS-*g*-PA6 was first *N*-trifluoroacetylated before the SEC [25].

2.4. Rheological characterization

An advanced rheometric expansion system (ARES) of type TA Instruments, USA, was used to characterize the rheological behavior of the pure polymer components and their blends. A dynamic mode was used to measure the complex viscosity as a function of frequency. The samples were disks of 25 mm in diameter and about 2 mm in thickness. The strain amplitude was set at 10% for all the measurements, which was in the range of the linear viscoelastic shear oscillation. The test was performed within the frequency range from 100 to 0.1 rad/s.

2.5. Solvent extraction

Solvent extraction was used to check if the PS/PA6 blends had a co-continuous structure or not. THF was used to dissolve out the PS or formic acid the PA6 at room temperature for 15 days, respectively. If the remaining phases, i.e., the PA6 phase after the THF extraction and PS phase after the formic acid extraction, were self-supporting without disintegration, they were considered as having a co-continuous morphology. The percentage of PS continuity was calculated based on the mass loss measurements before and after THF extraction:

$$\%\text{Continuity} = \frac{(\text{MassPS}_{\text{init}} - \text{MassPS}_{\text{final}})}{\text{MassPS}_{\text{init}}} \times 100 \quad (1)$$

2.6. Scanning electron microscopy

A scanning electron microscopy (SEM) of type FEI SIRION was used to characterize the blend morphologies. Before the SEM observations, samples were first fractured in liquid nitrogen. The fractured surfaces were then immersed in THF at room temperature for 12 h in order to etch the PS domains. They were dried for 12 h in a vacuum oven at 80 °C and then gold sputtered. The voltage for the SEM was 5.0 kV.

2.7. Mercury intrusion porosimetry

Mercury intrusion porosimetry techniques were used to characterize the microstructure of etched co-continuous blends and provided the pore diameter (D) [14,15]. It is based on the capillary law governing liquid penetration into small pores. This law, in the case of a non-wetting liquid like mercury and cylindrical pores, is expressed by the Washburn equation:

$$D = -\left(\frac{1}{P}\right) 4\gamma \cos\varphi \quad (2)$$

where P is the applied pressure, γ is the surface tension, and φ is the contact angle, all are in consistent units. The volume of mercury (V) penetrating the pores is measured directly as a function of applied pressure. This P–V information serves as a unique characterization of pore structure. The surface tension of mercury used here is 0.485 N/m. The contact angle between mercury and the solid is 130°.

Pores are rarely cylindrical. Hence the above equation constitutes a special model. Such a model may not best represent pores in actual materials, but its use is generally accepted as the practical means for treating what, otherwise, would be a most complex problem.

3. Results and discussion

3.1. Rheology

Fig. 1 shows the complex viscosity (η^*) at 230 °C of the PS, PA6 and their blends with a mass composition of 50/50 as a function of frequency. At low frequency, the complex viscosity of the PA6 was lower than that of the PS. That of the PS/PA6 blend was in between those of the PS and PA6, as expected. At high frequency, the complex viscosities of the PS, PA6 and their blend became close.

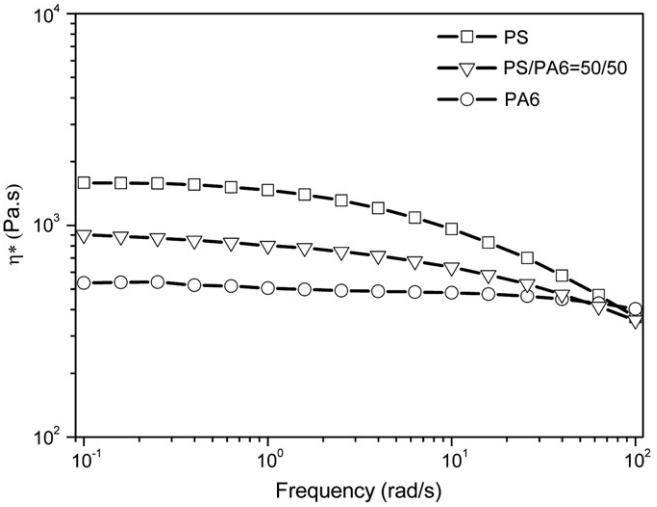

Fig. 1. Complex viscosity vs. frequency for the PS, PA6 and PS/PA6 blends (50/50) at 230 °C.

3.2. Annealing of blend systems without PS-g-PA6

Fig. 2 shows the SEM micrographs of the PS/PA6 (50/50) blend without PS-*g*-PA6 graft copolymer after quiescent annealing at different times (0, 5, 10 and 15 min) and different temperatures (230, 235 and 240 °C). Before the annealing the blend was a co-continuous structure (Fig. 2a). After the annealing, whatever the annealing time and/or temperature, the co-continuous morphology remained. This was also confirmed by the solvent extraction results. The latter showed that for all the samples before and after the annealing, the percentage of the PS continuity defined in Eq. (1) reached 100%. Moreover, after one phase was extracted out, the other phase was still self-supported. However, the pore size drastically increased with increasing annealing time and/or annealing temperature, indicating that a significant coarsening process had taken place. The fact that the pore size drastically increased while the co-continuous morphology remained is very interesting.

Fig. 3 shows the pore diameter (D) after the PS extraction in THF as a function of the annealing time for three different annealing temperatures. Both the annealing time and annealing temperatures had a big effect on the coarsening process. At 230 °C, D increased from 23 to 62 μm in 15 min; at 240 °C, it increased from 23 to 201 μm in 10 min. It is also noted that the pore size increased linearly with annealing time, whatever the annealing temperature. This is in agreement with the following two theories. The first one is an extension of a theory describing the disintegration of a cylinder thread immerged in another fluid, developed by Tomotika, to immiscible co-continuous blends. It was assumed that the coarsening rate dR/dt be directly related to the rate of growth of the distortion amplitude, $d\alpha/dt$ [14]. The growth of the average phase domain upon annealing was therefore governed by a capillary breakup process driven by interfacial tension, and a relation between phase size (D or R, the average pore diameter or radius) and annealing time (t) was finally obtained and expressed as:

$$\frac{D}{2} = R \sim kt \quad (3)$$

where k is the coarsening rate and is expressed as

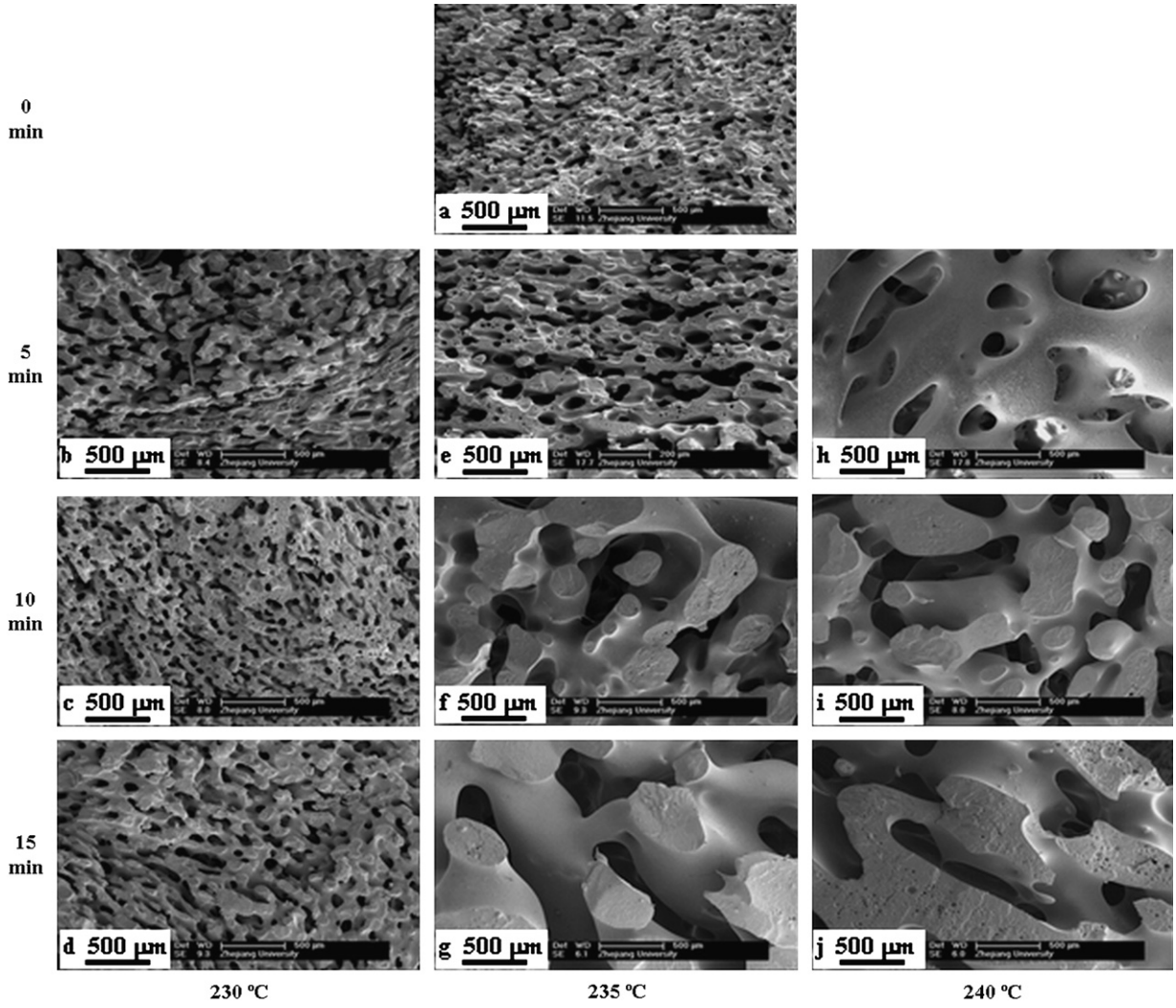

Fig. 2. Effect of the quiescent annealing on the morphology of the PS/PA6 (50/50) blend obtained after mixing at 100 rpm and at 230 °C for 10 min. Without annealing (a); annealing at 230 °C for 5 (b), 10 (c) and 15 min (d); annealing at 235 °C for 5 (e), 10 (f) and 15 min (g); annealing at 240 °C for 5 (h), 10 (i) and 15 min (j).

$$k = (\alpha_0/R_0)\frac{\sigma\Omega(\lambda,p)}{2\eta_c} \tag{4}$$

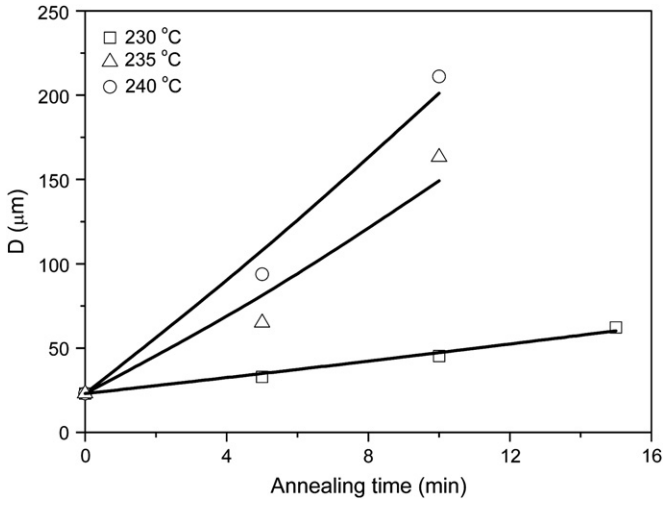

Fig. 3. Pore diameter (D) vs. annealing time for the PS/PA6 (50/50) blend at different annealing temperatures (230, 235 and 240 °C).

α_0/R_0 is the ratio of the original amplitude to the thread radius, σ is the interfacial tension, η_c is the viscosity of the continuous phase, and $\Omega(\lambda,p)$ is the Tomotika function related to the dominant wavelength, λ, and the viscosity ratio p ($p = \eta_d/\eta_c$, where η_d is the viscosity of the dispersed phase).

The second theory is an extension of the Doi–Ohta theory for complex interfaces to the annealing of co-continuous polymer blends [29]. The coarsening rate of co-continuous blends under quiescent annealing was expressed by:

$$\frac{1}{Q} = \frac{1}{Q_0} + c_1\frac{\sigma}{\eta}t \tag{5}$$

where Q_0 is the specific interfacial area at zero annealing time, c_1 is a kinetic constant for size relaxation, η is the viscosity of the polymer blend. The term $c_1\sigma/\eta$ represents the coarsening rate and $1/Q$ is proportional to R. Thus, these two theories indicate that at a given temperature, the coarsening rate is constant.

3.3. Annealing of polymer blends with PS-g-PA6

Fig. 4 compares the efficiency of three PS-*g*-PA6 graft copolymers (PS-*g*-PA6a, PS-*g*-PA6b and PS-*g*-PA6c) at stabilizing the morphology of the PS/PA6 (50/50) blend during annealing at 240 °C. Surprisingly, these blends did not have a co-continuous

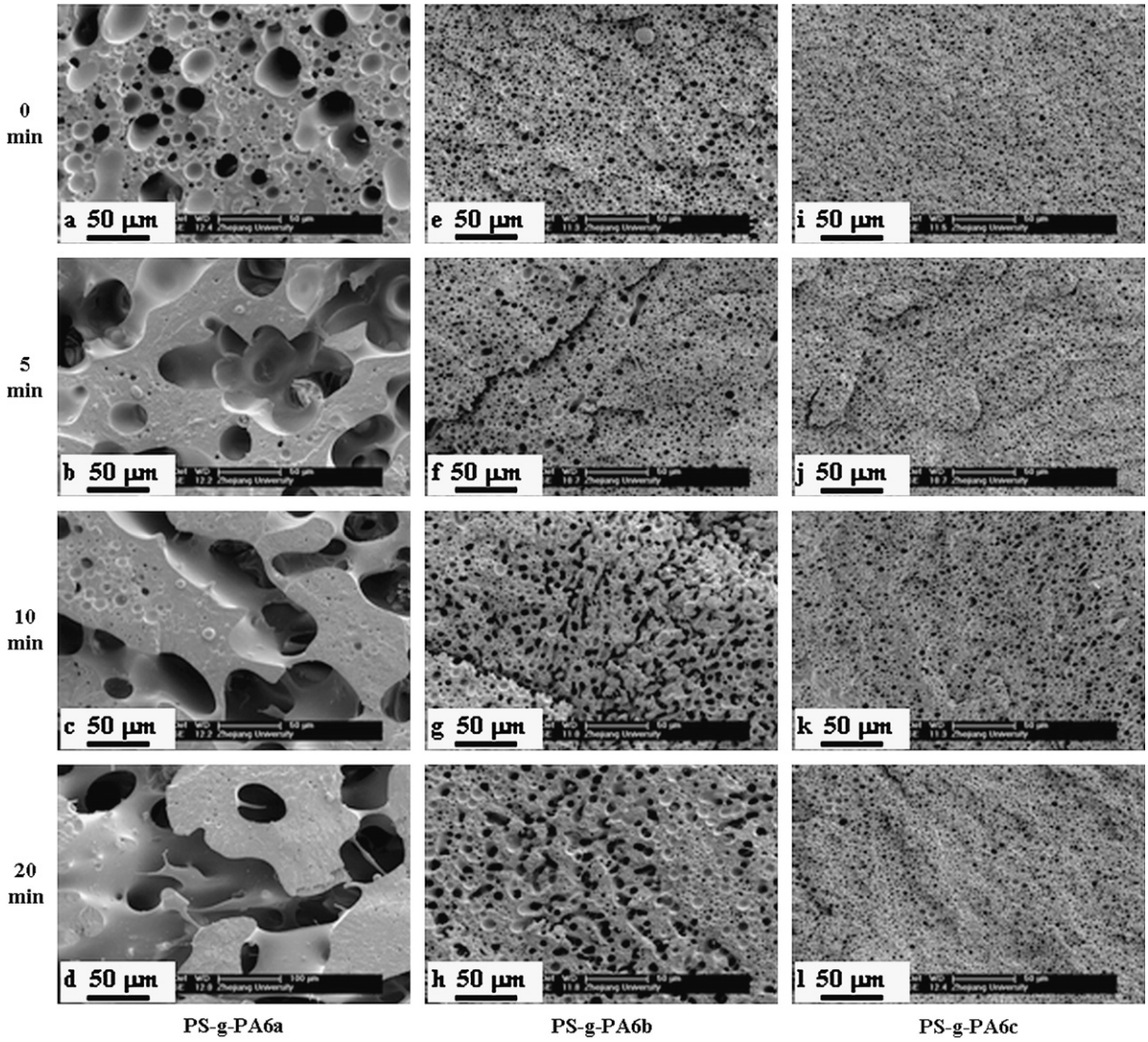

Fig. 4. SEM micrographs of PS/PA6/PS-*g*-PA6 (50/50/1) blends after mixing at 100 rpm for 10 min at 230 °C followed by annealing at 240 °C. The blend with PS-*g*-PA6a as the compatibilizer was annealed for 0 (a), 5 (b), 10 (c) and 20 min (d), respectively; the blend with PS-*g*-PA6b as the compatibilizer was annealed for 0 (e), 5 (f), 10 (g) and 20 min (h), respectively; the blend with PS-*g*-PA6c as the compatibilizer was annealed for 0 (i), 5 (j), 10 (k) and 15 min (l), respectively.

structure anymore. This is very different from the PS/PA6 (50/50) blend without PS-*g*-PA6. The solvent extraction showed that the region of co-continuity without and with 1 wt.% of PS-*g*-PA6 was from 40/60 to 65/35 (PS/PA6) and from 55/45 to 65/35, respectively, indicating that the addition of the PS-*g*-PA6 narrowed down the composition region of co-continuity. This is consistent with the literature results using block copolymers as compatibilizers [19–21]. It is also noted that the addition of PS-*g*-PA6 shifted the lower limit of the composition region of co-continuity to a higher PS/PA6 composition. However, it did not have a significant effect on its upper limit. This implies that in the presence of PS-*g*-PA6, the PA6 phase might have greater tendency to form the matrix than the PS phase. This could be explained as follows. First, the PA6 was likely less viscous than the PS under the blending conditions. The less viscous component has greater tendency to be the matrix [11,30,31]. Second, co-continuous structures of immiscible polymer blends are developed by droplet–droplet coalescence [4]. The presence of a copolymer reduces coalescence, stabilizes droplet morphologies and consequently disfavors the formation of co-continuous morphologies. In short, the above results seem to advise a rule that the addition of a compatibilizer tends to shift the lower limit of the co-continuity of the more viscous component to a higher value.

The size of dispersed phase of these three polymer blends before the annealing followed the order: PS-*g*-PA6a > PS-*g*-PA6b > PS-*g*-PA6c (Fig. 4(a,e and i, respectively)). After the annealing at 240 °C, the dispersed phase morphology with PS-*g*-PA6a as the compatibilizer tended to evolve into a co-continuous morphology and the domain size increased greatly. In the case of PS-*g*-PA6b, the dispersed phase morphology partly evolved into a co-continuous phase morphology and the domain size increased slightly. When PS-*g*-PA6c was used as the compatibilizer, the dispersed phase morphology was not subjected to any noticeable change. From the above results, the efficiency of PS-*g*-PA6 at suppressing coarsening followed the order: PS-*g*-PA6a < PS-*g*-PA6b < PS-*g*-PA6c. This implies that a PS-*g*-PA6 with longer grafts has higher compatibilizing and stabilizing efficiency. This is in line with their emulsifying efficiency for dispersed phase blends [32].

Fig. 5 shows the SEM micrographs of the PS/PA6 (60/40) blends before and after annealing at 240 °C and without PS-*g*-PA6 or with 1 wt.% of PS-*g*-PA6a, PS-*g*-PA6b, PS-*g*-PA6c or PS-*g*-PA6d as the compatibilizer. The compatibilizing and stabilizing efficiency

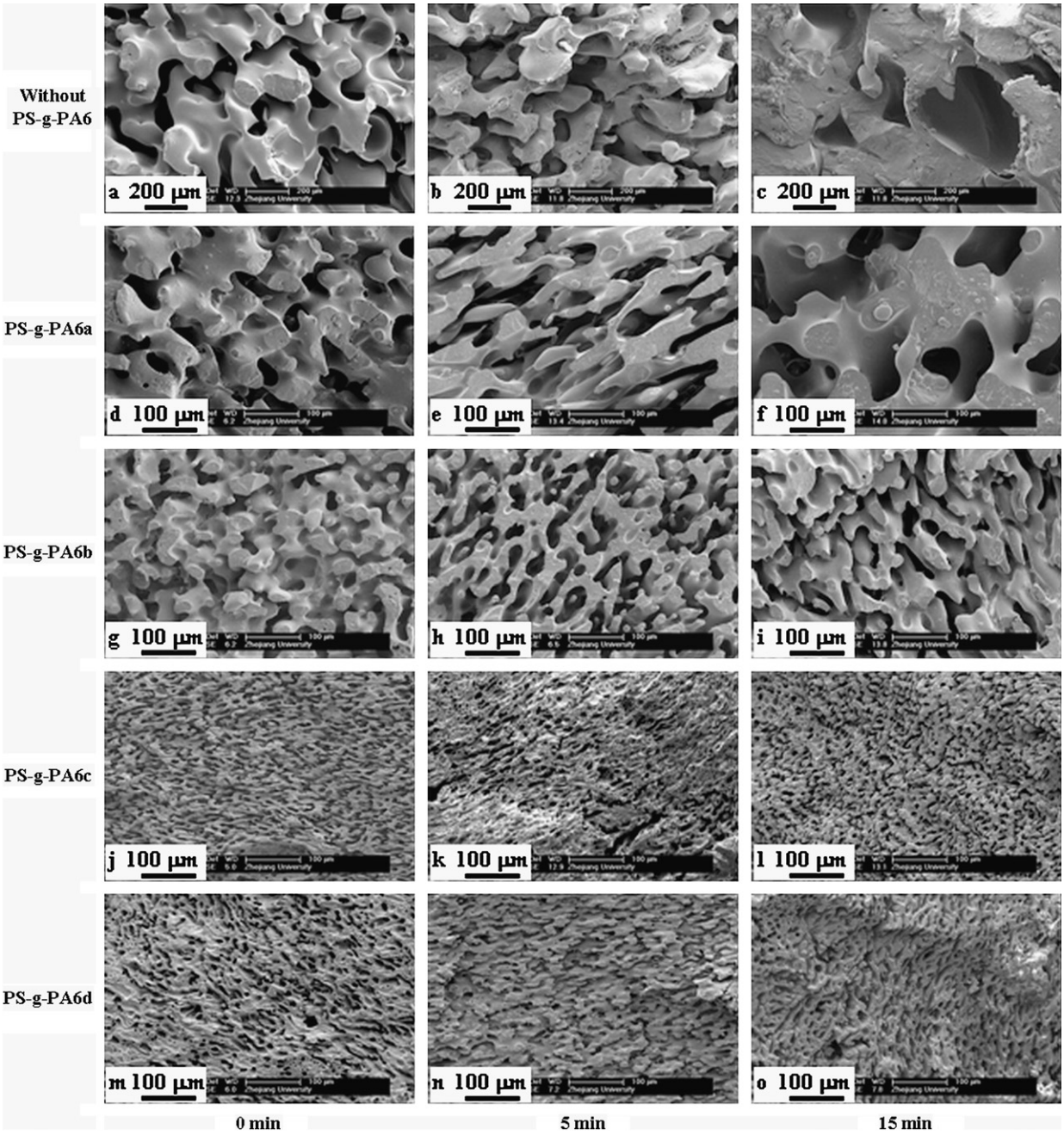

Fig. 5. Effect of adding 1 wt.% of PS-*g*-PA6 graft copolymer on the morphology of the PS/PA6 (60/40) blend after mixing at 100 rpm for 10 min at 230 °C followed by annealing at 240 °C. Without PS-*g*-PA6 and annealing for 0 (a), 5 (b) and 15 min (c), respectively; with PS-*g*-PA6a and annealing for 0 (d), 5 (e) and 15 min (f), respectively; with PS-*g*-PA6b and annealing for 0 (g), 5 (h) and 15 min (i), respectively; with PS-*g*-PA6c and annealing for 0 (j), 5 (k) and 15 min (l), respectively; with PS-*g*-PA6d and annealing for 0 (m), 5 (n) and 15 min (o).

followed the order: PS-*g*-PA6a $\ll$ PS-*g*-PA6b $<$ PS-*g*-PA6d $<$ PS-*g*-PA6c. Fig. 6 shows the pore diameter (D) of the above blends as a function of the annealing time. For the blends that contained 1 wt.% of PS-*g*-PA6a, D increased linearly with annealing time. In the case of PS-*g*-PA6b, D increased in size for the first 2 min and stopped increasing in size thereafter. As for PS-*g*-PA6c and PS-*g*-PA6d, D did not increase at all over the entire annealing time (20 min).

Fig. 7 is the schematic of the molecular architectures of the four PS-*g*-PA6 graft copolymers. Their PS backbones were almost the same in length and their PA6 grafts were different in length and/or in number of grafts per PS backbone. More specifically, PS-*g*-PA6a, PS-*g*-PA6b and PS-*g*-PA6c had the same PS backbone and number of grafts per PS backbone but differed in the PA6 graft length. As for PS-*g*-PA6d, both its PS backbone and PS/PA6 ratio were similar to those of PS-*g*-PA6b. However, the number of the PA6 grafts per PS backbone of the former was only half of the latter. Based on the above results, it can be concluded that for graft copolymers with similar backbone and graft chain number, the longer the grafts, the higher their compatibilizing and stabilizing efficiency. For a given backbone/graft composition, graft copolymers having fewer and longer grafts were more efficient at compatibilizing and stabilizing the co-continuous morphology.

The interface coverage (Σ) of copolymer, which is defined as the number of copolymer chains per unit area, has been used to understand the compatibilization efficiency of copolymers in

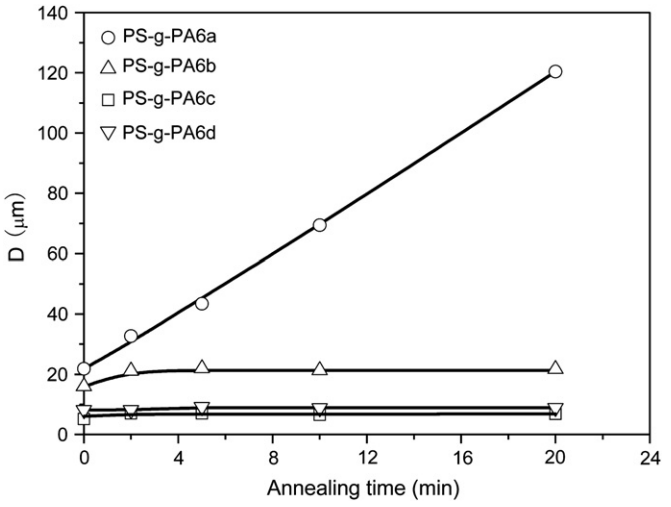

Fig. 6. Pore diameters of the PS/PA6/PS-*g*-PA6 (60/40/1) blends vs. annealing time at 240 °C. The compatibilizer was PS-*g*-PA6a, PS-*g*-PA6b, PS-*g*-PA6c and PS-*g*-PA6d, respectively.

immiscible polymer blends. For co-continuous blends it can be estimated by [33]:

$$\Sigma = \frac{w_{gcp}\rho_{PS}N_{av}D_{VS}}{6\phi_{PS}M_n} \quad (6)$$

where w_{gcp} is the mass fraction of the graft copolymer in the blends, ρ_{PS} is the density of homopolymer PS (0.934 g/cm^3 at 240 °C [34]), N_{av} is Avogadro's number, D_{VS} is the volume over surface area average diameter of a particle, ϕ_{PS} is the mass fraction of the PS phase and M_n is the number average molar mass of the graft copolymer. The values of M_n of PS-*g*-PA6 graft copolymers were estimated by SEC based on PS standards and are shown in Table 4. Eq. (6) was used to calculate Σ with the following assumptions. First, all the graft copolymers added to the blends resided at the interface between PS and PA6. Second, no micelles were formed in the blend systems. Third, the values of D_{vs} were equal to those of D obtained by the mercury intrusion porosimetry mentioned above. Table 5 shows the values of Σ.

The maximum interfacial coverage (Σ_{max}) can be estimated by assuming lamellar spacing of copolymer at the interface. However, the branched architecture of the graft copolymers can result in non-lamellar spacing due to asymmetric interfacial crowding. In our case, the concentration of branched graft copolymer necessary to saturate the interface can only be estimated by using a scaling relation $\Sigma_{max} \sim M_n^{-1/3}$ [22,35]. Jeon et al. [36] had estimated Σ_{max} values of 0.21 chain/nm^2 for a block copolymer of polystyrene and polyamide 66 (PS-*b*-PA66) with M_n of 77.0 kg/mol based on PS standards. Assuming that for a given M_n, PS-*g*-PA6 and PS-*b*-PA66 have the same Σ_{max} value for a given M_n, the Σ_{max} values are 0.23, 0.23, 0.21 and 0.23 chain/nm^2 for PS-*g*-PA6a, PS-*g*-PA6b, PS-*g*-PA6c and PS-*g*-PA6d, respectively. Table 5 shows the normalized interfacial coverage (Σ/Σ_{max}).

Table 5
Apparent interfacial coverage (Σ) and normalized interfacial coverage (Σ/Σ_{max}) for PS/PA6/PS-*g*-PA6 (60/40/1) blends before and after the annealing at 240 °C

Compatibilizer	Σ (chains/nm^2)		Σ/Σ_{max}	
	Before annealing	After 20 min annealing	Before annealing	After 20 min annealing
PS-*g*-PA6a	1.50	8.20	6.50	17.80
PS-*g*-PA6b	0.50	0.68	4.34	5.90
PS-*g*-PA6c	0.15	0.17	1.43	1.66
PS-*g*-PA6d	0.27	0.29	2.42	2.64

The ratio of Σ/Σ_{max} being above unity implies generally that a portion of copolymer existed in the bulk phases. For the blend with PS-*g*-PA6a, Σ/Σ_{max} increased from 6.50 to 17.80 during the annealing from 0 to 20 min. This indicates that a large portion of PS-*g*-PA6a was not at the interfaces before the annealing and that that portion increased during the annealing. The short PA6 grafts might have favored the formation of PS-*g*-PA6 micelles in the PS phase. In the case of PS-*g*-PA6b, the Σ/Σ_{max} value was 4.34 before the annealing and reached about 6 after 2 min of annealing. It did not increase anymore with further annealing. As for PS-*g*-PA6c and PS-*g*-PA6d, the Σ/Σ_{max} values increased only slightly during the annealing, indicating that the graft copolymer chains that were located in the interfaces prior to the annealing remained there during the annealing.

The interfacial thickness is also an important parameter for retarding coarsening during annealing. Noolandi and Hong [37,38] predicted that the longer chains of copolymer would increase the thickness of the interface, which would decrease the enthalpy of the system. Therefore, for graft copolymers with similar PS backbone and graft chain number, the longer the grafts of PS-*g*-PA6, the higher their compatibilizing and stabilizing efficiency. Kim and Jo [39] investigated the effect of the chain architecture of graft copolymers on the characteristic of an adsorbed layer on a surface using an off-lattice Monte Carlo simulation method. They found that when the mass ratio between the backbone and grafts is fixed, the layer thickness of a graft copolymer adsorbed onto the surface decreases with increasing the number of side chains. In other words, the chain conformation of the adsorbed polymer becomes more flattened as the length of the side chain becomes shorter. This implies that the graft chain length is more important for increasing the interfacial thickness than the graft chain density. This may explain the fact while PS-*g*-PA6b and PS-*g*-PA6d had almost the same PS/PA6 mass ratio, the latter exhibited much higher compatibilizing and stabilizing efficiency.

4. Conclusions

This work focused on the effect of adding a graft copolymer on the co-continuity of polymer blends, on the one hand, and their stability during quiescent annealing, on the other hand. The blends were composed of polystyrene (PS) and polyamide 6 (PA6). A series of graft copolymers of PS and PA6, denoted as PS-*g*-PA6, with different molecular structures were used as compatibilizers.

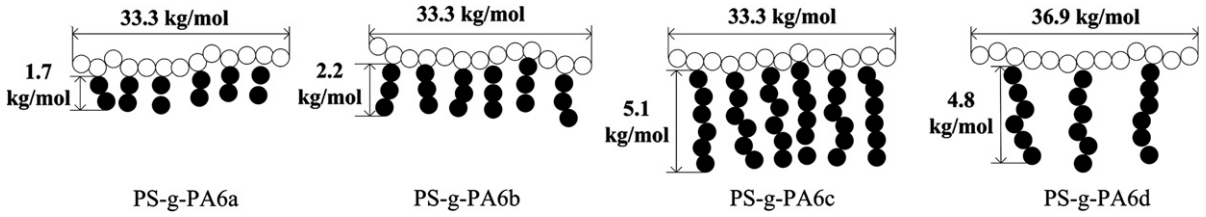

Fig. 7. Schematic of the molecular architectures and molar masses of the four PS-*g*-PA6 graft copolymers used in this work.

The addition of PS-*g*-PA6 narrowed the composition range of co-continuity of the PS/PA6 blend, from 40/60–65/35 (without PS-*g*-PA6) to 55/45–65/35 (with PS-*g*-PA6). In other words, it shifted the lower composition limit of co-continuity of the more viscous polymer component to a higher value.

Be compatibilized or not, a polymer blend with a co-continuous structure before annealing remained to be co-continuous after annealing. The presence of PS-*g*-PA6 reduced or stopped completely the coarsening of the co-continuous morphologies of the polymer blends, depending strongly on the molecular architecture (graft length and graft density) of the PS-*g*-PA6 graft copolymer. For graft copolymers with the same backbone and the number of grafts per backbone, the longer the grafts, the higher their compatibilizing and stabilizing efficiency. For a given backbone/graft mass ratio, the longer the grafts and concomitantly the smaller the number of grafts per backbone, the higher the compatibilizing and stabilizing efficiency of the PS-*g*-PA6 graft copolymer.

Acknowledgments

The authors thank the National Natural Science Foundation of China (grant numbers 50390097 and 20310285), the Ministry of Science and Technology of China through an international cooperation program (grant number: 2001CB711203) and the Association Franco-Chinoise pour la Recherche Scientifique et Technique – AFCRST (grant number: PRA Mx02-07) for their financial support.

References

[1] Willemse RC, Boer AP, Dam JV, Gotsis AD. Polymer 1999;40:827.
[2] Bhadane PA, Champagne MF, Huneault MA, Tofan F, Favis BD. J Polym Sci Part B Polym Phys 2006;44:1919.
[3] Bhadane PA, Champagne MF, Huneault MA, Tofan F, Favis BD. Polymer 2006;47:2760.
[4] Li J, Ma PL, Favis BD. Macromolecules 2002;35:2005.
[5] Sarazin P, Favis BD. Polymer 2005;46:5966.
[6] Pernot H, Baumert M, Court F, Leibler L. Nat Mater 2002;1:54.
[7] Bhanu N, Kandpal LD, Mathur GN. J Appl Polym Sci 2003;90:2887.
[8] Arns CH, Knackstedt MA, Roberts AP, Pinczewski VW. Macromolecules 1999;32:5964.
[9] Meincke O, Kaempfer D, Weickmann H, Friedrich C, Vathauer M, Warth H. Polymer 2004;45:739.
[10] Li Y, Hiroshi S. Macromol Rapid Commun 2005;26:710.
[11] Lee JK, Han CD. Polymer 1999;40:2521.
[12] Willemse RC. Polymer 1999;40:2175.
[13] Mekhilef N, Favis BD, Carreau PJ. J Polym Sci Part B Polym Phys 1997;35:293.
[14] Yuan Z, Favis BD. AIChE J 2005;51:271.
[15] Yuan Z, Favis BD. J Polym Sci Part B Polym Phys 2006;44:711.
[16] Baker W, Scott C, Hu GH. Reactive polymer blending. Munich: Hanser Publisher; 2001.
[17] Li T, Hiltner A, Baer E, Qurik RP. J Polym Sci Part B Polym Phys 1995;33:667.
[18] Li H, Hu GH, Sousa JA. J Polym Sci Part B Polym Phys 1999;37:3368.
[19] Bourry D, Favis BD. J Polym Sci Part B Polym Phys 1998;36:1889.
[20] Dedecher K, Groeninckx G. Polymer 1998;39:4993.
[21] Chuai CZ, Almdal K, Lyngaae-Jørgensen J. Polymer 2003;44:481.
[22] Galloway JA, Jeon HK, Bell JR, Macosko CW. Polymer 2005;46:183.
[23] Harrats C, Blacher S, Fayt R, Jérôme R, Teyssié Ph. J Polym Sci Part B Polym Phys 1995;33:801.
[24] Harrats C, Fayt R, Jérôme R, Blacher S. J Polym Sci Part B Polym Phys 2003;41:202.
[25] Zhang CL, Feng LF, Gu XP, Hoppe S, Hu GH. Polym Test 2007;26:699.
[26] Zhang CL, Feng LF, Hu GH, Xu ZB. J Appl Polym Sci 2006;101:1972.
[27] Zhang CL, Feng LF, Hoppe S, Hu GH. J Polym Sci Part A Polym Chem 2008;46:4766.
[28] Li GZ, Feng LF, Gu XP, Xu ZB, Hu GH, Liu JH. Funct Polym 2005;18:127.
[29] Vinckier I, Laun HM. J Rheol 2001;45:1373.
[30] Jafari SH, Pötschke P, Stephan M, Warth H, Alberts H. Polymer 2002;43:6985.
[31] Willemse RC, Boer AP, Dam JV, Gotsis AD. Polymer 1998;39:5879.
[32] Zhang CL, Feng LF, Gu XP, Hoppe S, Hu GH. Polymer 2007;48:5940.
[33] Jeon HK, Zhang JB, Macosko CW. Polymer 2005;46:12422.
[34] Brandrup J, Immergut EH, editors. Polymer handbook. 4th ed.; 1998.
[35] Omonov TS, Harrats C, Groeninckx G, Moldenaers P. Polymer 2007;48:5289.
[36] Jeon HK, Feist BJ, Koh SB, Chang K, Macosko CW, Dion RP. Polymer 2004;45:197.
[37] Noolandi J, Hong MK. Macromolecules 1982;15:482.
[38] Noolandi J, Hong MK. Macromolecules 1984;17:1531.
[39] Kim KH, Jo WH. Polymer 2001;42:3205.